Residual depth migration

The preceding two chapters describe two wavefront propagation methods for calculating the traveltimes and geometrical amplitudes of seismic waves. These methods can also calculate the gradient fields of traveltime and take-off angle. This chapter extends these methods and results to a new application — residual depth migration.

Residual depth migration is a process of converting an image migrated with one interval velocity model to an image migrated with another. As noted in Chapter ??, each iteration of depth-migration velocity analysis involves the processes of estimating the perturbations of the interval velocities and then remigrating the data with the updated velocity model. However, complete remigration in each iteration is computationally expensive. When the perturbations of the interval velocities are small, residual depth migration can be considerably more efficient than full depth migration. The high efficiency results from the partial focusing effect of the previous migration. If the depth migration is implemented by the Kirchhoff integral, then the partial focusing effect makes the aperture of the residual depth migration operator smaller than that of the full depth migration operator. Consequently, the application of the residual migration operator needs fewer arithmetic operations. However, calculating the operator for residual depth migration is generally difficult when the interval velocities vary spatially.

This chapter describes an efficient algorithm for calculating the Kirchhoff integral operator of residual depth migration. This algorithm can be applied when both the initial interval velocities and their perturbations vary spatially. Also it is generally applicable to both post-stack and prestack migration, and to both common-shot and constant-offset geometries. This chapter begins with a theoretical discussion in which I derive an integral formula for residual depth migration. This formula involves two mapping functions that are defined in a system of nonlinear equations. Next, I introduce an efficient algorithm for solving the nonlinear system to obtain the residual depth migration operator. I then briefly explain how to apply the operator to data. Finally, I use synthetic examples to demonstrate the residual depth migration algorithm.

Theory of residual depth migration

For the sake of simplicity, the theory is presented for a 2-D medium and a line source. It can easily be revised for a point source by referring to the corresponding theory of depth migration (Deregowski, 1985; Etgen, 1990).

Kirchhoff depth migration

A scalar wave field $P(t, x_s, x_g)$ is recorded in an area that has a subsurface structure $Q(x, z)$ and a velocity model $v(x, z)$, where t is the time interval starting from the firing of the shot, x_s and x_g are the shot and geophone coordinates along the survey line, and (x, z) are the coordinates of a subsurface position. Deregowski (1985) shows that this wave field can be modeled by the Kirchhoff integral, as follows:

$$P(t, x_s, x_g) = \int_x \int_z R_{s,g} A_s A_g D_{\frac{1}{2}}(t) * w(t) * \delta(t - \tau_s - \tau_g) Q(x, z) dx dz, \qquad (1)$$

where $*$ stands for the convolution in time, $R_{s,g}$ is a directivity function, $D_{\frac{1}{2}}(t)$ is the impulse response of the half-derivative operator, $w(t)$ is a source wavelet, and $A_c = A(x, z; x_c)$ and $\tau_c = \tau(x, z; x_c)$ for $c = s$ or g are the geometrical amplitude and traveltime functions, respectively, with a source at the surface position x_c. Deregowski (1985) also shows that

$$R_{s,g} = \frac{1}{2}(\cos\theta_s + \cos\theta_g), \qquad (2)$$

where θ_s and θ_g are the open angles of the incident ray and the reflection ray to the normal of a reflector at (x, z), respectively.

For an individual common-shot gather or constant-offset section, the migration operator is approximated by the conjugate of the modeling operator (Claerbout, 1992). Therefore the image migrated from a gather or section can be formulated as follows:

$$Q(x, z; \eta) = \int_\xi \int_t R_{s,g} A_s A_g \delta(t - \tau_s - \tau_g) w(t) \odot D_{\frac{1}{2}}(t) \odot P(t, x_s, x_g) dt d\xi, \qquad (3)$$

where $\odot$ stands for the cross-correlation in time. For common-shot migration, $\xi = x_g$ and $\eta = x_s$; for constant-offset migration, $\xi = 0.5(x_g + x_s)$ and $\eta = 0.5(x_g - x_s)$. The final image of the subsurface structure is estimated by stacking the migrated gathers or sections as follows:

$$Q(x, z) = \frac{1}{N(x, z)} \int_\eta Q(x, z; \eta) d\eta, \qquad (4)$$

where $N(x, z)$ is a weighting function

$$N(x, z) = \int_t \int_{x_s} \int_{x_g} (R_{s,g} A_s A_g)^2 \delta(t - \tau_s - \tau_g) dt dx_s dx_g.$$

For the given velocity model $v(x, z)$, the geometrical amplitude and traveltime functions are computed by the wavefront propagation methods developed in Chapters 2 and 3. The Kirchhoff depth migration is accomplished by implementing the integrals in equations (3) and (4) numerically.

Integral formulation of residual depth migration

If an individual gather or section is migrated with a wrong velocity model $\hat{v}(x, z)$, the image obtained, $\hat{Q}(\hat{x}, \hat{z}; \eta)$, is distorted from the correct image, $Q(x, z; \eta)$. Similarly to equation (3), one has

$$\hat{Q}(\hat{x}, \hat{z}; \eta) = \int_\xi \int_t \hat{R}_{s,g} \hat{A}_s \hat{A}_g \delta(t - \hat{\tau}_s - \hat{\tau}_g) w(t) \odot D_{\frac{1}{2}}(t) \odot P(t, x_s, x_g) dt d\xi, \qquad (5)$$

where $\hat{A}_c = \hat{A}(\hat{x}, \hat{z}; x_c)$ and $\hat{\tau}_c = \hat{\tau}(\hat{x}, \hat{z}; x_c)$ for $c = s$ or g are the geometrical amplitude and traveltime functions computed from the velocity model $\hat{v}(\hat{x}, \hat{z})$, respectively.

Residual depth migration is a linear transformation from the distorted image $\hat{Q}(\hat{x}, \hat{z}; \eta)$ to the correct image $Q(x, z; \eta)$. In Appendix B, I show that such a linear transformation can be approximated by an integral as follows:

$$Q(x, z; \eta) = \int_\xi [R_{s,g} A_s A_g \hat{R}_{s,g} \hat{A}_s \hat{A}_g B(0) \hat{Q}(\hat{x}, \hat{z}; \eta)] \Big|_{\substack{\hat{x} \;=\; \hat{x}(x,z;\xi) \\ \hat{z} \;=\; \hat{z}(x,z;\xi)}} d\xi. \tag{6}$$

Here $B(0)$ is an autocorrelation function, and $\hat{x} = \hat{x}(x, z; \xi)$ and $\hat{z} = \hat{z}(x, z; \xi)$ are mapping functions that are implicitly expressed in the following system of nonlinear equations:

$$\begin{cases} \tau(x, z; x_s) + \tau(x, z; x_g) = \hat{\tau}(\hat{x}, \hat{z}; x_s) + \hat{\tau}(\hat{x}, \hat{z}; x_g) \\ p(x, z; x_s) \dfrac{\partial x_s}{\partial \xi} + p(x, z; x_g) \dfrac{\partial x_g}{\partial \xi} = \hat{p}(\hat{x}, \hat{z}; x_s) \dfrac{\partial x_s}{\partial \xi} + \hat{p}(\hat{x}, \hat{z}; x_g) \dfrac{\partial x_g}{\partial \xi}, \end{cases} \tag{7}$$

where p and $\hat{p}$ are the surface horizontal slownesses defined as follows:

$$\begin{cases} p(x, z; x_c) = \dfrac{\partial \tau}{\partial x_c} = \dfrac{\sin \gamma_c}{v(x_c, 0)} \\ \hat{p}(\hat{x}, \hat{z}; x_c) = \dfrac{\partial \hat{\tau}}{\partial x_c} = \dfrac{\sin \hat{\gamma}_c}{\hat{v}(x_c, 0)}, \end{cases} \tag{8}$$

Here, $\gamma_c = \gamma(x, z; x_c)$ and $\hat{\gamma}_c = \hat{\gamma}(x, z; x_c)$ are the take-off angles of the rays starting at the surface position x_c and ending at subsurface positions (x, z) and $(\hat{x}, \hat{z})$, respectively. The take-off angles are measured from the vertical.

The partial derivatives of x_s and x_g with respect to ξ are determined in the following way. For post-stack sections,

$$\frac{\partial x_s}{\partial \xi} = \frac{\partial x_g}{\partial \xi} = 1.$$

For common-shot gathers,

$$\frac{\partial x_s}{\partial \xi} = 0 \quad \text{and} \quad \frac{\partial x_g}{\partial \xi} = 1.$$

For constant-offset sections,

$$\frac{\partial x_s}{\partial \xi} = 1 \quad \text{and} \quad \frac{\partial x_g}{\partial \xi} = 1.$$

Therefore, equation (7) is generally applicable. A similar equation was derived and used by Etgen (1990) for residual migration of constant-offset sections with constant velocities. It was also used by Van Trier (1990) for residual event migration.

Figure 1 explains equation (7) graphically. A seismic event at horizontal position ξ and arrival time τ of a time section has a time dip p. The time dip is the derivative of τ with respect to ξ. Migration with two different velocity models $v(x,z)$ and $\hat{v}(\hat{x},\hat{z})$ gives two images of the reflector that generates the event. These two images are located at (x,z) and $(\hat{x},\hat{z})$, respectively. The kinematics of residual depth migration is defined by the mapping between the image location (x,z) and the image location $(\hat{x},\hat{z})$. The mapping functions can be determined through the modeling of the kinematic parameters of the event. Because the images at (x,z) and $(\hat{x},\hat{z})$ are migrated from the same event, equation (7) states that the arrival time and time dip computed from the reflector at (x,z) with velocity model $v(x,z)$ are identical to those computed from the reflector at $(\hat{x},\hat{z})$ with velocity model $\hat{v}(\hat{x},\hat{z})$.

Calculating operators by the finite difference method

The key step in calculating the residual-depth-migration operators is to find the mapping functions. For each fixed ξ, equation (7) implicitly defines the mapping from an image location $(\hat{x},\hat{z})$ on $\hat{Q}(\hat{x},\hat{z};\eta)$ to an image location (x,z) on $Q(x,z;\eta)$. To find the mapping functions for the given velocity models $v(x,z)$ and $\hat{v}(\hat{x},\hat{z})$, the system of nonlinear equations has to be solved by using a numerical method. Searching is a straightforward method in which for each point (x,z) all points around it are checked to find the point $(\hat{x},\hat{z})$ that satisfies equation (7) (Van Trier, 1990). However, this algorithm becomes time consuming when the dimensions of images are large.

This section describes an algorithm that solves equation (7) using finite-difference techniques. The ideas are similar to those of the wavefront propagation methods described in Chapters **??** and **??**. The nonlinear system (7) is first converted to a system of linear partial differential equations. With the assumption that two models $v(x,z)$ and $\hat{v}(\hat{x},\hat{z})$ have the same near-surface velocities, the solutions to the nonlinear system are known to be $\hat{x}=x$ and $\hat{z}=z$ near the surface. These solutions are then extrapolated by solving the partial differential equations.

Conversion to partial differential equations

To solve equation (7) through an extrapolation process, we need to have a system of partial differential equations that consist of the following partial derivatives:

$$\frac{\partial \hat{x}}{\partial x}, \qquad \frac{\partial \hat{z}}{\partial x}, \qquad \frac{\partial \hat{x}}{\partial z} \quad \text{and} \quad \frac{\partial \hat{z}}{\partial z}.$$

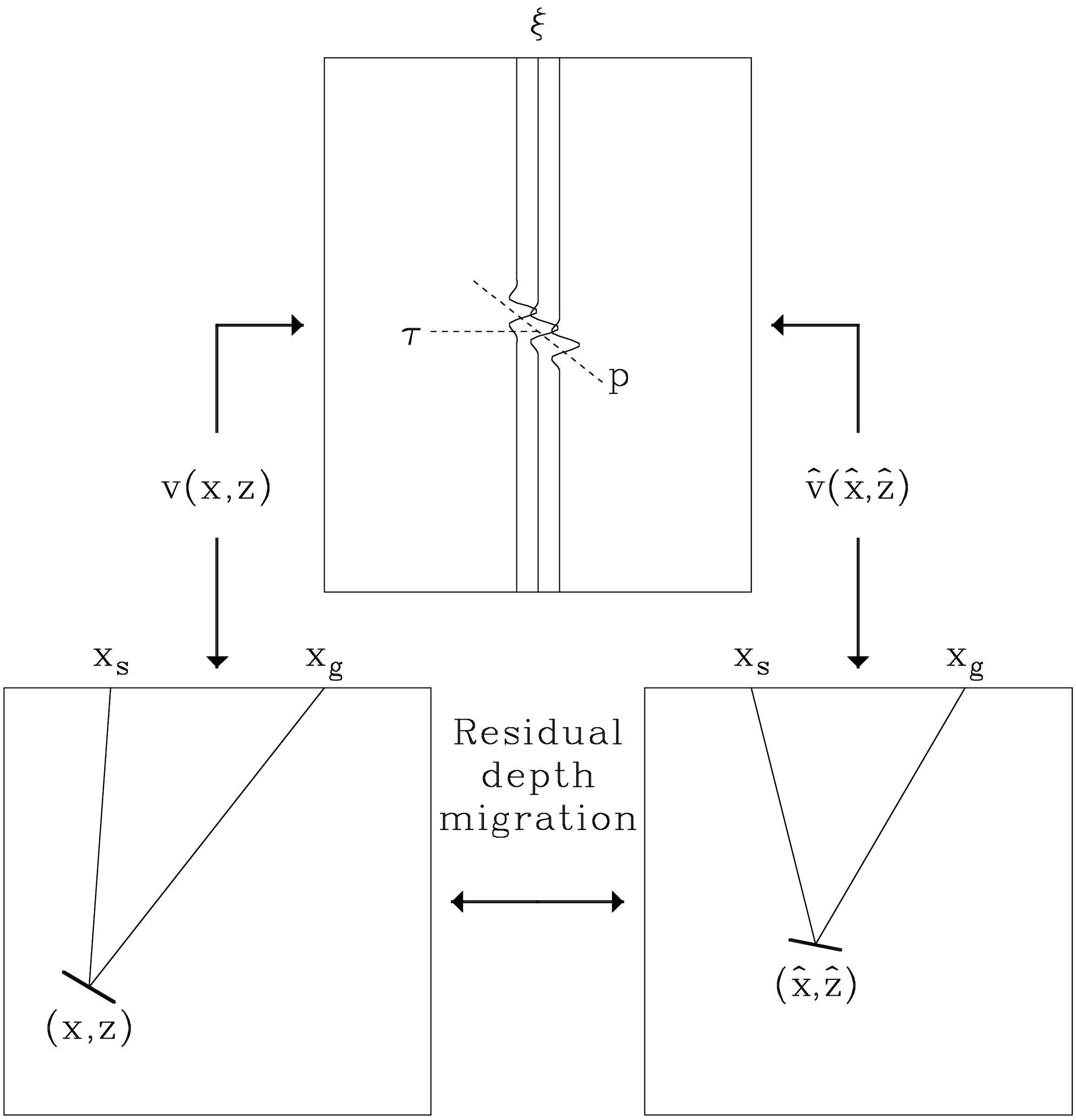

Figure 1: A graphic illustration of residual depth migration. resmig4-vprmig [ER]

Let us first simplify notation by denoting

$$\begin{aligned}
M(x,z,x_s,x_g) &= \tau(x,z;x_s)+\tau(x,z;x_g)\\
N(x,z,x_s,x_g) &= p(x,z;x_s)\frac{\partial x_s}{\partial \xi}+p(x,z;x_g)\frac{\partial x_g}{\partial \xi}\\
\hat{M}(\hat{x},\hat{z},x_s,x_g) &= \hat{\tau}(\hat{x},\hat{z};x_s)+\hat{\tau}(\hat{x},\hat{z};x_g)\\
\hat{N}(\hat{x},\hat{z},x_s,x_g) &= \hat{p}(\hat{x},\hat{z};x_s)\frac{\partial x_s}{\partial \xi}+\hat{p}(\hat{x},\hat{z};x_g)\frac{\partial x_g}{\partial \xi}.
\end{aligned}$$

Equation (7) then becomes

$$\left\{\begin{aligned}
M(x,z,x_s,x_g) &= \hat{M}(\hat{x},\hat{z},x_s,x_g)\\
N(x,z,x_s,x_g) &= \hat{N}(\hat{x},\hat{z},x_s,x_g).
\end{aligned}\right. \tag{9}$$

Taking partial derivatives of both sides of this system of nonlinear equations with respect to x and z, respectively, and rearranging the terms yields

$$\begin{pmatrix} \hat{M}_{\hat{x}} & \hat{M}_{\hat{z}} \\ \hat{N}_{\hat{x}} & \hat{N}_{\hat{z}} \end{pmatrix} \begin{pmatrix} \dfrac{\partial \hat{x}}{\partial x} \\ \dfrac{\partial \hat{z}}{\partial x} \end{pmatrix} = \begin{pmatrix} M_x \\ N_x \end{pmatrix} \tag{10}$$

and

$$\begin{pmatrix} \hat{M}_{\hat{x}} & \hat{M}_{\hat{z}} \\ \hat{N}_{\hat{x}} & \hat{N}_{\hat{z}} \end{pmatrix} \begin{pmatrix} \dfrac{\partial \hat{x}}{\partial z} \\ \dfrac{\partial \hat{z}}{\partial z} \end{pmatrix} = \begin{pmatrix} M_z \\ N_z \end{pmatrix}, \tag{11}$$

where subscripts x, z, $\hat{x}$, and $\hat{z}$ denote partial derivatives with respect to x, z, $\hat{x}$, and $\hat{z}$, respectively. Solving these linear equation sets analytically gives two sets of partial differential equations for $(\hat{x},\hat{z})$:

$$\left\{\begin{aligned}
\frac{\partial \hat{x}}{\partial x} &= \frac{M_x\hat{N}_{\hat{z}}-\hat{M}_{\hat{z}}N_x}{\hat{M}_{\hat{x}}\hat{N}_{\hat{z}}-\hat{M}_{\hat{z}}\hat{N}_{\hat{x}}}\\
\frac{\partial \hat{z}}{\partial x} &= \frac{\hat{M}_{\hat{x}}N_x-M_x\hat{N}_{\hat{x}}}{\hat{M}_{\hat{x}}\hat{N}_{\hat{z}}-\hat{M}_{\hat{z}}\hat{N}_{\hat{x}}},
\end{aligned}\right. \tag{12}$$

and

$$\left\{\begin{aligned}
\frac{\partial \hat{x}}{\partial z} &= \frac{M_z\hat{N}_{\hat{z}}-\hat{M}_{\hat{z}}N_z}{\hat{M}_{\hat{x}}\hat{N}_{\hat{z}}-\hat{M}_{\hat{z}}\hat{N}_{\hat{x}}}\\
\frac{\partial \hat{z}}{\partial z} &= \frac{\hat{M}_{\hat{x}}N_z-M_z\hat{N}_{\hat{x}}}{\hat{M}_{\hat{x}}\hat{N}_{\hat{z}}-\hat{M}_{\hat{z}}\hat{N}_{\hat{x}}}.
\end{aligned}\right. \tag{13}$$

The right sides of these equations contain the partial derivatives of M, N, $\hat{M}$ and $\hat{N}$. These partial derivatives are related to the partial derivatives of traveltimes and surface horizontal slownesses as follows:

$$
\begin{aligned}
\hat{M}_{\hat{x}} &= \hat{\tau}_{\hat{x}}(\hat{x},\hat{z};x_s)+\hat{\tau}_{\hat{x}}(\hat{x},\hat{z};x_g) & \hat{M}_{\hat{z}} &= \hat{\tau}_{\hat{z}}(\hat{x},\hat{z};x_s)+\hat{\tau}_{\hat{z}}(\hat{x},\hat{z};x_g)\\
M_x &= \tau_x(x,z;x_s)+\tau_x(x,z;x_g) & M_z &= \tau_z(x,z;x_s)+\tau_z(x,z;x_g)\\
\hat{N}_{\hat{x}} &= \hat{p}_{\hat{x}}(\hat{x},\hat{z};x_s)\frac{\partial x_s}{\partial \xi}+\hat{p}_{\hat{x}}(\hat{x},\hat{z};x_g)\frac{\partial x_g}{\partial \xi} & \hat{N}_{\hat{z}} &= \hat{p}_{\hat{z}}(\hat{x},\hat{z};x_s)\frac{\partial x_s}{\partial \xi}+\hat{p}_{\hat{z}}(\hat{x},\hat{z};x_g)\frac{\partial x_g}{\partial \xi}\\
N_x &= p_x(x,z;x_s)\frac{\partial x_s}{\partial \xi}+p_x(x,z;x_g)\frac{\partial x_g}{\partial \xi} & N_z &= p_z(x,z;x_s)\frac{\partial x_s}{\partial \xi}+p_z(x,z;x_g)\frac{\partial x_g}{\partial \xi}.
\end{aligned}
$$

With equations (12) and (13), the mapping functions $\hat{x}=\hat{x}(x,z;\xi)$ and $\hat{z}=\hat{z}(x,z;\xi)$ can be extrapolated in either the horizontal or the vertical direction. Since the mapping functions are usually known near the surface, equation (13) is used to extrapolate them vertically down to each depth.

An alternative approach is to transform the nonlinear system (7) into polar coordinates (r,θ). The system of partial differential equations

$$
\left\{
\begin{aligned}
\frac{\partial \hat{\theta}}{\partial r} &= \frac{M_r N_{\hat{r}} - M_{\hat{r}} N_r}{M_{\hat{\theta}} N_{\hat{r}} - M_{\hat{r}} N_{\hat{\theta}}}\\
\frac{\partial \hat{r}}{\partial r} &= \frac{M_{\hat{\theta}} N_r - M_r N_{\hat{\theta}}}{M_{\hat{\theta}} N_{\hat{r}} - M_{\hat{r}} N_{\hat{\theta}}}
\end{aligned}
\right. \tag{14}
$$

can be used to extrapolate the mapping functions in the radial direction. If the gradient fields of traveltime and surface horizontal slowness are calculated in polar coordinates, extrapolation in the radial direction is easy to implement.

The gradient field of traveltime

For a given interval velocity model, the traveltime field can be calculated on a regular grid by using the wavefront propagation methods presented in Chapters **??** and **??**. If the finite difference method is used, two components of the gradient field in polar coordinates (r,θ) can be approximated by

$$
\left\{
\begin{aligned}
\tau_r(r_j,\theta_i;x_c) &\approx 0.5(w_{i,j}+w_{i,j-1})\\
\frac{1}{r_j}\tau_\theta(r_j,\theta_i;x_c) &\approx 0.5(u_{i,j}+u_{i-1,j}),
\end{aligned}
\right. \tag{15}
$$

where

$$
w_{i,j} = \frac{\tau(r_{j+1},\theta_i;x_c)-\tau(r_j,\theta_i;x_c)}{\Delta r}
$$

and

$$
u_{i,j} = \frac{\tau(r_j,\theta_{i+1};x_c)-\tau(r_j,\theta_i;x_c)}{r_j\Delta\theta}.
$$

As noted in Chapter **??**, the finite-difference approximation to the traveltime-gradient calculation is valid only when the velocity model is reasonably smooth. If the given model contains large velocity contrasts, a 2-D smoothing filter must be applied to the model before the calculation is conducted. The two-point averaging in equation (15) also aims to reduce the noise caused by the finite-difference approximation.

The local ray-tracing method described in Chapter **??** computes the traveltime-gradient field directly on a regular grid in the Cartesian coordinates (x, z). Because the method uses a smooth velocity representation, it gives more accurate gradient fields than does the finite-difference method.

The gradient field of surface horizontal slowness

The surface horizontal slowness of wave propagation is related to the take-off angle of the associated ray as follows:

$$p = \frac{\partial \tau}{\partial x_c} = \frac{\sin \gamma_c}{v_c}, \tag{16}$$

where v_c and γ_c are the velocity and the take-off angle at the surface position x_c, respectively, so

The finite-difference method presented in Chapter **??** computes the take-off angle field on a regular grid in polar coordinates. Two components of the gradient field of take-off angle are approximated by

$$\left\{ \begin{array}{lcl} \gamma_r(r_j, \theta_i; x_c) & \approx & 0.5(g_{i,j} + g_{i,j-1}) \\ \\ \dfrac{1}{r_j}\gamma_\theta(r_j, \theta_i; x_c) & \approx & 0.5(f_{i,j} + f_{i-1,j}), \end{array} \right. \tag{17}$$

where

$$g_{i,j} = \frac{\gamma(r_{j+1}, \theta_i; x_c) - \gamma(r_j, \theta_i; x_c)}{\Delta r}$$

and

$$f_{i,j} = \frac{\gamma(r_j, \theta_{i+1}; x_c) - \gamma(r_j, \theta_i; x_c)}{r_j \Delta \theta}.$$

In the process of wavefront propagation through local ray-tracing, the partial derivatives of the take-off angle with respect to the ray-centered coordinates (s, n) are calculated on a regular grid in the Cartesian coordinate system. They are

$$\left\{ \begin{array}{lcl} \dfrac{\partial \gamma}{\partial s} & = & 0 \\ \\ \dfrac{\partial \gamma}{\partial n} & = & J, \end{array} \right. \tag{18}$$

where s is the arc-length of the center ray, n is the normal distance to the center ray, and J is the Jacobian of the transformation from Cartesian coordinates to ray coordinates (see Chapter 3 for details). Two components of the gradient field in Cartesian coordinates are determined by

$$\begin{cases} \dfrac{\partial \gamma}{\partial x} = \dfrac{\partial \gamma}{\partial s}\dfrac{\partial s}{\partial x} + \dfrac{\partial \gamma}{\partial n}\dfrac{\partial n}{\partial x} = Jv\tau_z \\ \\ \dfrac{\partial \gamma}{\partial z} = \dfrac{\partial \gamma}{\partial s}\dfrac{\partial s}{\partial z} + \dfrac{\partial \gamma}{\partial n}\dfrac{\partial n}{\partial z} = Jv\tau_x, \end{cases} \tag{19}$$

where $v = v(x, z)$ is the interval velocity at the subsurface point (x, z). Once the gradient field of take-off angle is calculated, equation (??) is used to compute the gradient field of surface horizontal slowness.

Extrapolation by the finite difference method

Now that the gradient fields of traveltime and surface horizontal slowness can be calculated, the next step is to solve equation (13) or (14) with proper initial conditions. Take equation (14) as an example. The calculations are conducted in the polar coordinate system whose origin is at the surface position ξ. With the assumption that two given velocity models are identical near the surface, the initial conditions are set to be

$$\begin{cases} \hat{r} = r \\ \\ \hat{\theta} = \theta \end{cases} \qquad \text{for} \quad r \le r_0, \tag{20}$$

where r_0 is the maximum radius of a circle centered at surface position ξ within which two given velocity models are identical. Starting from these initial conditions, we can extrapolate the mapping functions $\hat{r} = \hat{r}(r, \theta)$ and $\hat{\theta} = \hat{\theta}(r, \theta)$ in the radius direction as follows:

$$\begin{cases} \hat{r}_{j+1} = \hat{r}_j + \left[\dfrac{\partial \hat{r}}{\partial r}\right]_j \Delta r \\ \\ \hat{\theta}_{j+1} = \hat{\theta}_j + \left[\dfrac{\partial \hat{\theta}}{\partial r}\right]_j \Delta r, \end{cases} \tag{21}$$

where j is the index of the grid in the radial direction. The results are then mapped onto an even grid in the Cartesian coordinate system.

Although a sophisticated, higher-order Runge-Kutta methods for solving equation (14) are available (Press et al., 1986), the simple scheme expressed in equation (21) is accurate enough for structural imaging if the initial interval velocity model and the velocity perturbations are smooth. Fortunately, in practice, smooth velocity models are normally used for depth migration. This is because high-wavenumber components of the true velocity model of the earth may not be accurately estimated from conventional surface reflection data, which have limited frequency bandwidths. Using an inaccurate velocity model containing sharp contrasts in depth migration may yield an erroneous image.

Applying operators to migrated images

Compared with the calculation of the operators, the application of the operators to migrated images is relatively simple. The integral in equation (6) is numerically implemented as the following summation:

$$Q(x,z;\eta) = \sum_k [R_{s,g} A_s A_g \hat{R}_{s,g} \hat{A}_s \hat{A}_g B(0) \hat{Q}(\hat{x},\hat{z};\eta)] \Big|_{\substack{\hat{x} \;=\; \hat{x}(x,z;\xi_k) \\ \hat{z} \;=\; \hat{z}(x,z;\xi_k)}} \Delta\xi_k, \qquad (22)$$

where $\Delta\xi_k$ is the sampling interval along the ξ axis. Because the aperture of a residual-depth-migration operator is smaller than that of the corresponding full-depth-migration operator, the sampling interval $\Delta\xi_k$ used for residual depth migration can be chosen to be several times greater than that used for full depth migration. Therefore, with the same surface coverage, fewer arithmetic operations are needed for computing the summation in equation (22). This explains why residual depth migration is computationally economic.

A synthetic example

The following example illustrates the residual depth migration of zero-offset sections with a structural velocity model. The model, shown in Figure 2, consists of several dipping layers and a low-velocity cap over a high-velocity dome. I calculated the traveltime field in this model using the finite-difference method described in Chapter **??**, and generated the synthetic data using Kirchhoff modeling. Figure 3 shows a zero-offset time-section generated from a reflectivity model consisting of twelve scatterers. The energy diffracted from each scatterer is distributed along a diffraction curve. Migrating this time-section with a constant velocity of 2 km/s produces a depth section shown in Figure 3. Because the velocity model used in migration differs from the true velocity model, the energies diffracted from the scatterers in the lower part of the model are not completely focused, nor are they positioned correctly. The partially focused energy are distributed along curves which I call residual diffraction curves. The residual diffraction curves vary spatially because of the the variations of interval velocities. Their apertures are smaller than that of the diffraction curves on the unmigrated time-section. The kinematic operators of residual depth migration are defined along these residual diffraction curves. I calculated the residual depth-migration operators by the finite-difference method described in this chapter. Overlain on the bottom panel of Figure 3 are kinematic operators that correspond to the four scatterers of the middle column. I then applied residual depth migration to the initially migrated depth-section. The result is shown in Figure 4. After residual depth migration, the images of all scatterers are well focused and positioned.

Figure 5 shows a zero-offset section generated from a reflectivity model. The reflectivity model is constructed from the interfaces of the velocity model shown in Figure 2. Migration with a constant velocity of 2 km/s yields the depth image displayed in Figure 5. The images of shallow reflectors are positioned correctly because the interval velocities in these layers are close to the constant migration velocity. On the other hand, the images of the deep reflectors are seriously mispositioned because the interval velocities in these layers are considerably higher than the migration velocity. The low-velocity cap causes the images of the bottom of the dome to be flattened. However, after residual depth migration, as shown in Figure 6, the positional distortion of the images of the reflectors are completely corrected.

Summary

This chapter described an algorithm for residual depth migration of reflection seismic data in general varying velocity media. The algorithm consists of two steps: (1) calculating the operators through an extrapolation process, (2) applying the calculated operators to initially migrated images. This algorithm is generally applicable to both poststack and prestack migration, and to both common-shot and constant-offset geometries. The application to a synthetic example demonstrates that the algorithm can correct the positional distortion of the image migrated with a wrong velocity model.

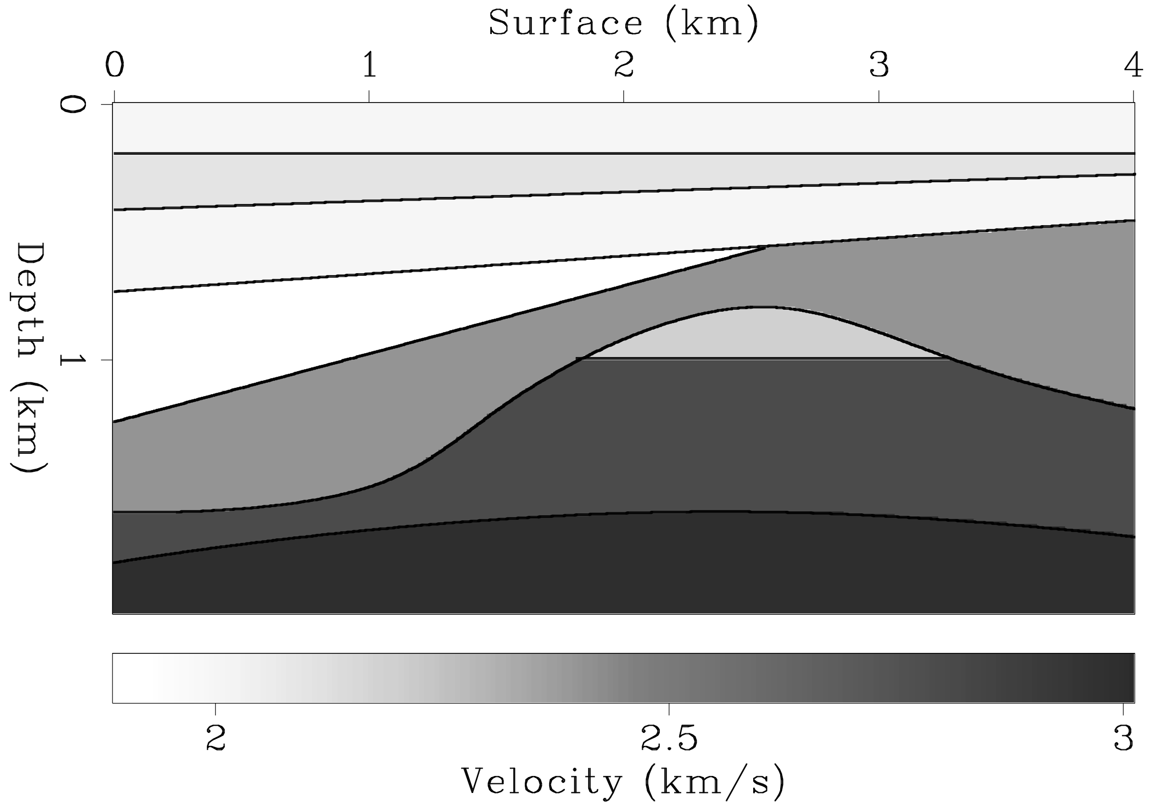

Figure 2: A synthetic interval velocity model. High intensity represents high velocity. The solid curves indicate the boundaries of layers. resmig4-velsyn [ER]

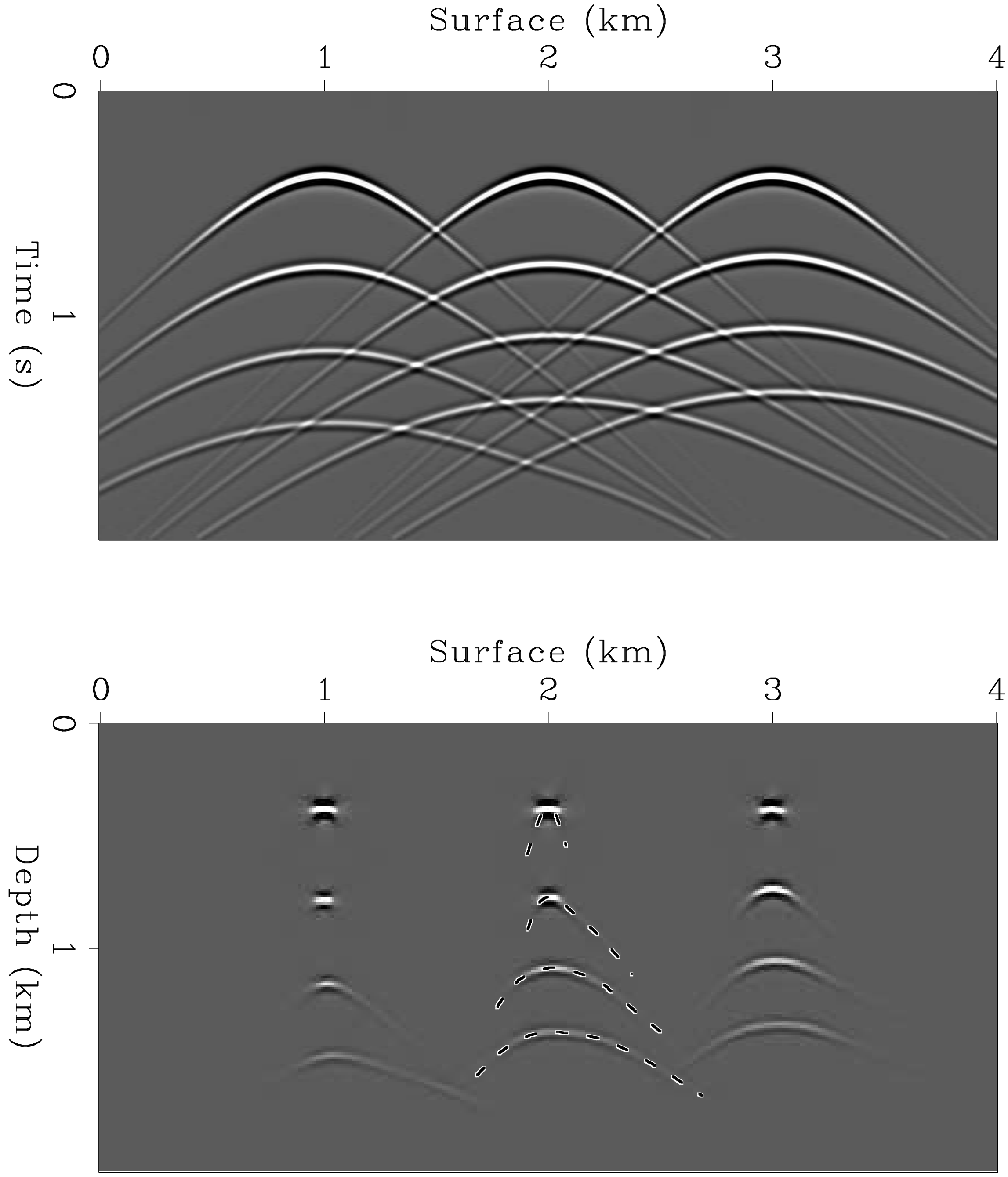

Figure 3: The top panel shows the synthetic zero-offset section generated by Kirchhoff modeling. The reflectivity model contains twelve scatterers. The traveltime field is computed from the synthetic interval velocity model shown in Figure 2. The bottom panel shows the results of migration with a constant velocity equal to the surface velocity. Overlain are the kinematic operators of residual depth migration, calculated by the finite-difference method. resmig4-datspk [ER]

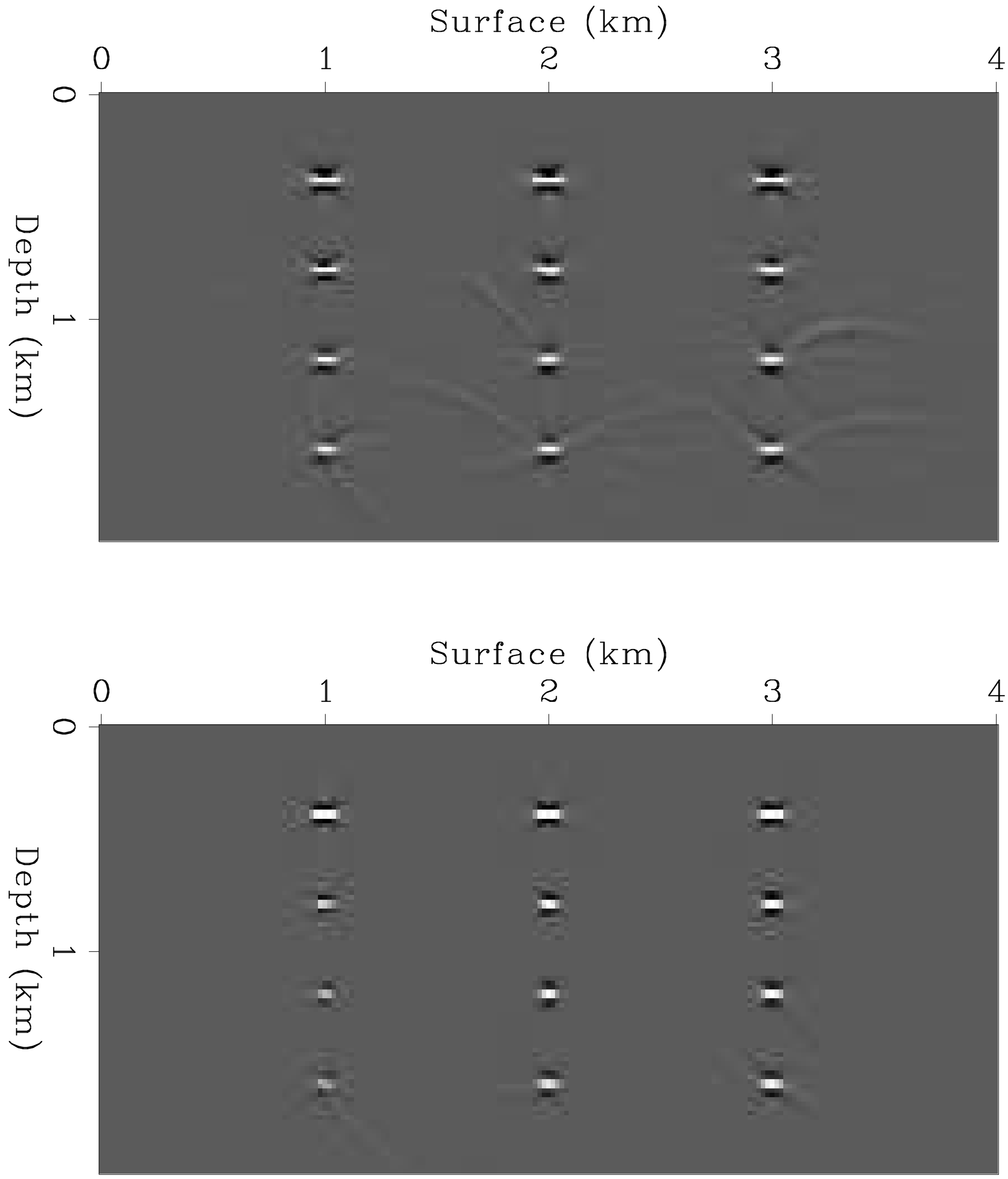

Figure 4: The top panel shows the image of the scatterers after residual depth migration. For comparison, the bottom panel shows the image obtained by full migration with the correct interval velocity model. resmig4-imgspk [ER]

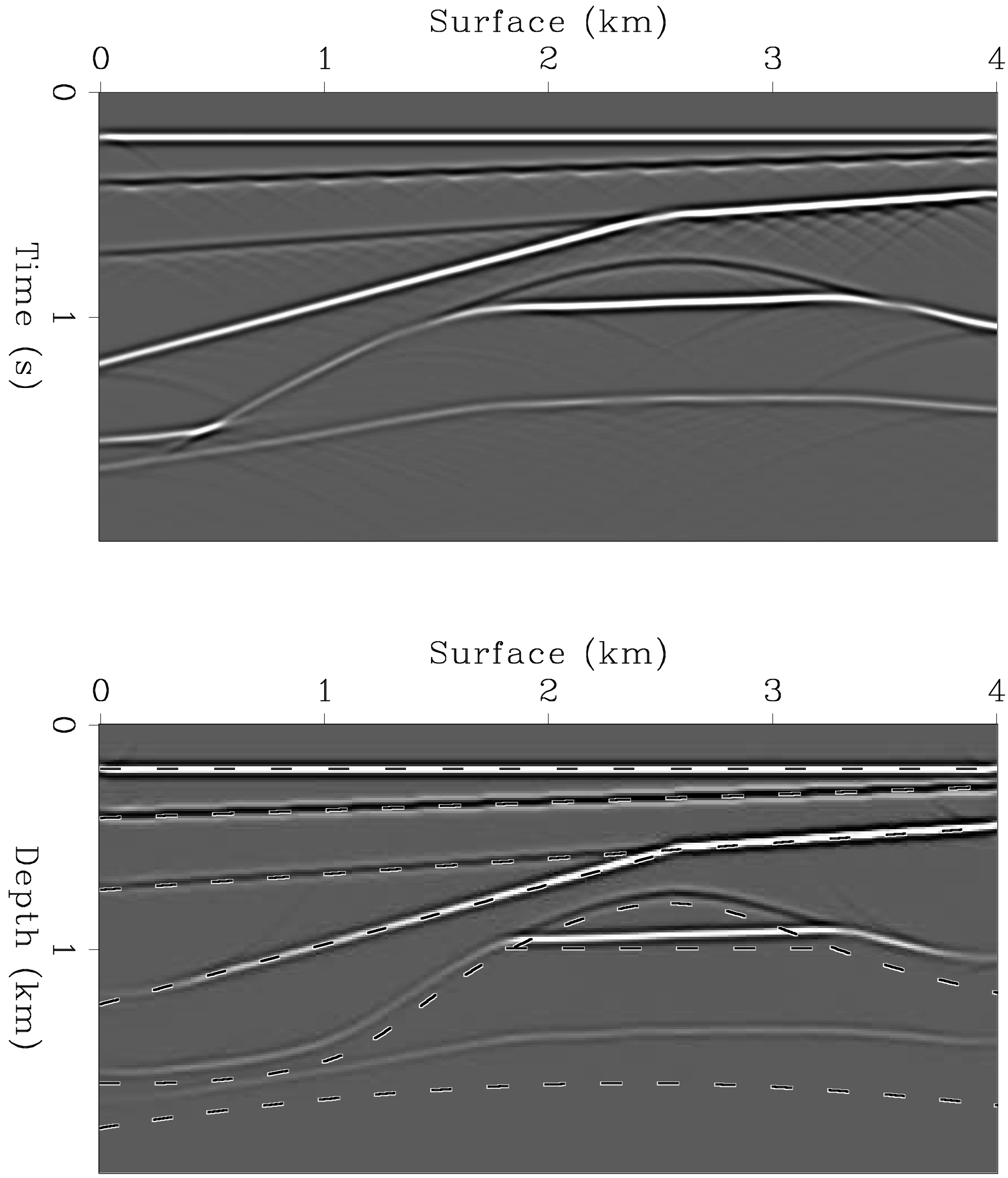

Figure 5: The top panel shows the synthetic zero-offset section generated from the synthetic velocity model. The bottom panel shows the resul of migration with a constant velocity equal to the surface velocity. resmig4-datsyn [ER]

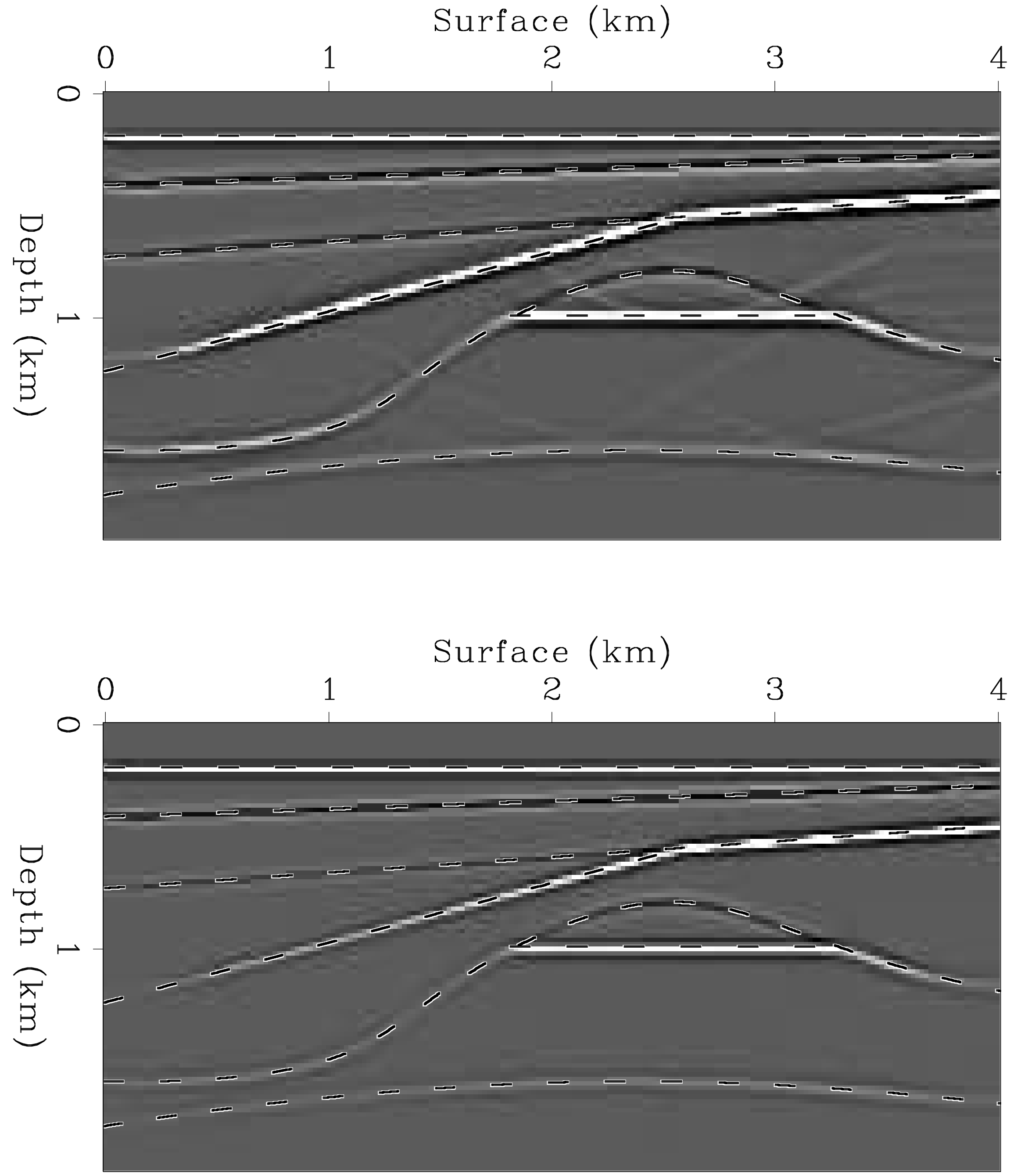

Figure 6: The top panel shows the image after residual depth migration. For comparison, the bottom panel shows the image obtained by full migration with the correct interval velocity model. The dashed curves indicates the true positions of the interfaces. resmig4-imgsyn [ER]